Point source atom interferometry with a cloud of finite size

Gregory W. Hoth,[a)] Bruno Pelle, Stefan Riedl, John Kitching, and Elizabeth A. Donley

National Institute of Standards and Technology, Boulder, Colorado 80305, USA

We demonstrate a two axis gyroscope by the use of light pulse atom interferometry with an expanding cloud of atoms in the regime where the cloud has expanded by 1.1–5 times its initial size during the interrogation. Rotations are measured by analyzing spatial fringe patterns in the atom population obtained by imaging the final cloud. The fringes arise from a correlation between an atom's initial velocity and its final position. This correlation is naturally created by the expansion of the cloud, but it also depends on the initial atomic distribution. We show that the frequency and contrast of these spatial fringes depend on the details of the initial distribution and develop an analytical model to explain this dependence. We also discuss several challenges that must be overcome to realize a high-performance gyroscope with this technique.
[http://dx.doi.org/10.1063/1.4961527]

Over the last few decades, light-pulse atom interferometers (LPAIs) have proven their outstanding sensitivity and stability for inertial measurements.[1] These sensors are now making their way out of the laboratory into field demonstrations. Transportable LPAIs have realized accelerometry in a zero-g plane flight,[2] precision gravimetry,[3–5] gravity gradiometry,[6] and measurements of the Earth's rotation.[7] However, applications such as inertial navigation will need systems that are smaller, lighter, and require lower power than the mobile systems demonstrated so far. This will require new techniques optimized for use in a compact volume.

Most LPAI inertial sensors use a $\pi/2 - \pi - \pi/2$ pulse sequence.[8] In this scheme, accelerations, $\vec{a}$, and rotations, $\vec{\Omega}$, produce phase shifts given by[9]

$$\Phi_a = \vec{k}_{\text{eff}} \cdot \vec{a}\, T_R^2, \tag{1}$$

$$\Phi_\Omega = 2\vec{k}_{\text{eff}} \cdot (\vec{\Omega} \times \vec{v}) T_R^2, \tag{2}$$

where $\vec{k}_{\text{eff}}$ is the effective wave-vector for the Raman transitions, $\vec{v}$ is the velocity of the atoms, and T_R is the time between consecutive pulses.

In order to realize a sensor, we must have a method to distinguish these two phase shifts. This is typically done by combining the signals from two interferometers with counter-propagating atoms.[10] With this technique, LPAIs based on thermal beams[10,11] and laser cooled atoms[12–14] have demonstrated performance that exceeds the requirements for navigation-grade gyroscopes, which can be loosely defined[11,15] as a short term rotation sensitivity of $1\,\text{mdeg}/\sqrt{h}$, a bias stability of $1\,\text{mdeg/h}$, and a scale factor stability of 1×10^{-6}. However, the use of multiple atomic sources comes at the cost of significantly increasing the size and complexity of these systems.

Recently, it has been shown that it is possible to isolate Φ_Ω using a single cloud of atoms by imaging the cloud after the interferometer sequence. This technique, dubbed point source interferometry (PSI) by Dickerson *et al.*,[9] exploits the correlation between the position and velocity created by the expansion of the cloud. When the final size of the cloud is much larger than its initial size, each atom's final position, $\vec{r}$, is essentially determined by its initial velocity, $\vec{v}$. This allows the approximation $\vec{r} \approx \vec{v}\, T_{\text{ex}}$ where T_{ex} is the total expansion time. In this point source limit, Eq. (2) becomes $\Phi_\Omega = \vec{k}_\Omega \cdot \vec{r}$ with

$$\vec{k}_\Omega = 2T_R^2(\vec{k}_{\text{eff}} \times \vec{\Omega})/T_{\text{ex}} = F_{\text{ps}}\,\Omega\,\hat{n}. \tag{3}$$

Here, $\hat{n}$ is a unit vector perpendicular to both $\vec{\Omega}$ and $\vec{k}_{\text{eff}}$ and $F = k_\Omega/\Omega$ is a scale factor. For a point source, the scale factor is $F_{\text{ps}} = 2T_R^2 k_{\text{eff}}/T_{\text{ex}}$. We have assumed $\vec{\Omega} \cdot \vec{k}_{\text{eff}} = 0$ for simplicity. We have also neglected the Raman momentum kick and gravity because the rotation phase shift depends on the atoms' transverse velocity while these effects change the component of $\vec{v}$ along the direction of k_{eff}, assuming $\vec{g} \parallel \vec{k}_{\text{eff}}$. If $\vec{g}$ is not parallel to $\vec{k}_{\text{eff}}$, a constant phase shift would be produced, but the phase gradient, Eq. (3), would not change.

In the point source limit, the rotation phase shift becomes a phase gradient described by Eq. (3), which will produce a spatial fringe pattern in the state of the atoms. For an interferometer based on Raman transitions, the output states correspond to different hyperfine states, and so these fringes can be imaged with state-selective detection. If k_{eff} is in the z direction and the image plane is the $x - y$ plane, then a_z, Ω_x, and Ω_y can be determined from Eqs. (1) and (3) by analyzing the orientation, frequency, and phase of the fringe pattern.

PSI offers both a much simpler set-up than methods based on multiple atomic sources and efficient use of the evacuated volume. It seems to be a promising tool for compact LPAI sensors. However, in a compact system, the expansion time will be limited by the size of the device, and it is likely that the point source approximation will not be valid. To address this issue, we have developed a model for the PSI fringes when the cloud has a finite initial size. This can be done by treating the initial cloud as a sum of many point sources. The first step is to describe the evolution of one point source.

Consider an infinitesimally small cloud of N two level atoms with temperature T. At $t = 0$, the cloud begins to expand. During the expansion, a $\pi/2 - \pi - \pi/2$ pulse sequence is

a)Electronic mail: gregory.hoth@nist.gov

applied. At $t = T_{ex} = 2T_R + T_d$, the density distribution is imaged. Here, T_d represents delays due to experimental details such as the initial state preparation. The point source will have evolved into a Gaussian spatial distribution with a final width $\sigma_{f,ps} = T_{ex}\sqrt{k_B T/m}$. Due to the interferometer, the state of the atoms will be modulated by a fringe described by k_Ω. The density distribution of one of the output states is given by

$$n_{ps}(\vec{r}) = \frac{N \exp\left(-\frac{\vec{r}^2}{2\sigma_f^2}\right)}{(2\pi)^{\frac{3}{2}}\sigma_f^3} \frac{\left(1 + c\cos\left(\vec{k}_\Omega \cdot \vec{r} + \Phi_a\right)\right)}{2}, \quad (4)$$

where c is the interferometer contrast.

Now consider the same experiment with an initial cloud described by a density profile $n_0(\vec{r})$ and temperature T. In this case, the final cloud can be modeled as a sum of all the expanded point sources that make up the initial cloud. Formally, this means that the final density distribution is given by the convolution of $n_0(\vec{r})$ with the expanded point source from Eq. (4)

$$n_f(\vec{r}, T_{ex}) = n_0(\vec{r}) * n_{ps}(\vec{r}, T_{ex}). \quad (5)$$

As a first approximation, we consider the case where the initial density distribution is a Gaussian with a characteristic width σ_0. In this case, Eq. (5) can be evaluated analytically. The final density profile is a Gaussian modulated by fringes that is formally identical to Eq. (4). However, the final cloud size, the phase gradient, and the fringe contrast are all modified. The phase gradient still takes the form $\vec{k}_\Omega = F\Omega\hat{n}$, but the scale factor becomes

$$F_g = F_{ps}(1 - (\sigma_0^2/\sigma_f^2)), \quad (6)$$

where $\sigma_f = \sqrt{\sigma_0^2 + (k_B T/m)T_{ex}^2}$ is the width of the final cloud. The spatial fringe contrast decreases with Ω as

$$c(\Omega) = c_0 \exp\left(-F_{ps}^2\Omega^2\sigma_0^2(1 - \sigma_0^2/\sigma_f^2)/2\right), \quad (7)$$

where c_0 is the interferometer contrast with $\Omega = 0$.

The connection between the contrast and the initial size comes about because our detection method is only sensitive to the final position of the atoms. When the cloud has a finite initial size, atoms with different initial velocities and therefore different phase shifts will end up at the same final position. We average over this distribution of phase shifts, which washes out the fringes.

The relationship between the scale factor and the initial size is also due to the imperfect correlation between the atoms' initial velocities and their final positions. In general, each point r in the expanded cloud contains atoms that are both slower and faster than $v_{ps} = r/T_{ex}$. For a Gaussian initial cloud, there are more atoms with $v < v_{ps}$ which means that the average velocity at each point in the expanded cloud is lower than it would be if the initial cloud were a point source. Thus, the detected phase gradient is lower for the Gaussian initial cloud. As the cloud expands, the correlation between the position and velocity builds up; in the limit $\sigma_f \gg \sigma_0$, we recover the point source scale factor.

The connection between the initial distribution and the scale factor predicted by this model represents a significant systematic effect for a PSI gyroscope and so it is important to confirm it experimentally. We investigate this effect with a LPAI based on cold Rb atoms. Our setup has been previously described,[16] so we will only briefly review it here. Cold atoms are produced by the use of a standard vapor-cell magneto-optical trap (MOT) in an uncoated cell with a 1 cm × 1 cm cross-section. The MOT is formed 1 cm above the bottom wall of the cell, which limits the free expansion time to $T_{ex} \approx 50$ ms. The atom interferometer is realized by driving stimulated Raman transitions[8] between the $|F = 1, m_F = 0\rangle$ and $|F = 2, m_F = 0\rangle$ ground states of ^{87}Rb. The Raman beams are incident from the top of the cell. One beam is retro-reflected to drive the counter-propagating Raman transition while the other beam is coupled out by the use of a polarizing beam splitter. This beam path is used to image a plane orthogonal to $\vec{k}_{eff}$. Rotations are simulated[9,17] by tilting the retro-reflection mirror for the Raman beam at a rate Ω. This set up is illustrated schematically in Fig. 1.

In each run of the experiment, we load 8×10^6 ^{87}Rb atoms in 2 s. This long loading time is undesirable for a sensor, but it is not important for our study of the scale factor. In a fully optimized system, the cycle time could be reduced to 50 ms with the use of atom recapture.[18] After loading the MOT, the atoms are cooled to $T \approx 5\,\mu$K by the use of optical molasses. The atoms are then optically pumped to $|F = 1, m_F = 0\rangle$ and allowed to fall for 10 ms in order to separate the co- and counter-propagating Raman transitions. The co-propagating transition is present due to reflections from the uncoated cell. After this initial free fall, a $\pi/2 - \pi - \pi/2$ pulse sequence is applied with a π pulse duration of 6 μs. The time between consecutive pulses, T_R, is varied from 2 ms to 16 ms. Absorption imaging is used to measure the density distribution of the atoms in $|F = 2\rangle$ and the total population. The time elapsed between the two images is 250 μs. From these two images, the ratio $R = (2N_{F=2} - N_{tot})/N_{tot}$ is calculated.
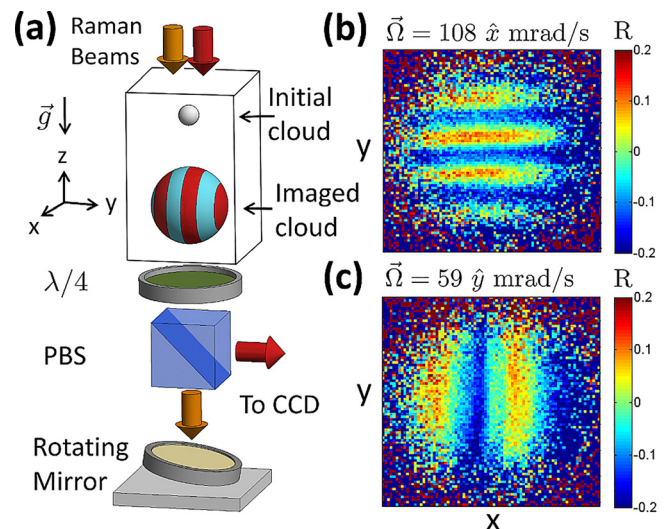

FIG. 1. (a) Diagram of our set up illustrating the geometry for interrogation and imaging. (b), (c) PSI fringes with $T_R = 8$ ms and $T_{ex} = 28.3$ ms. We plot $R = (2N_{F=2} - N_{tot})/N_{tot}$ to cancel out the cloud shape. Each image corresponds to one shot. The images are 4 × 4 mm.

This approximately cancels out the cloud shape and reveals the PSI fringes as shown in Fig. 1.

Although the fringes can be clearly seen, it is difficult to determine the phase gradient k from images like those shown in Fig. 1 because of imperfect cancellation of the cloud shape, due to the expansion of the cloud between the two images, and because of spatial variation of the interferometer contrast, due to intensity variation in our Raman beams. In order to estimate k, we take many shots with the same Ω while varying the overall interferometer phase by perturbing the gravity-compensating frequency ramp between the Raman lasers. The phase is scanned over four fringes in 100 shots. By tracking an individual pixel through this set of images and fitting a sinusoid, the fringe contrast, offset, and phase are determined as a function of position. An example phase map is shown in Fig. 2. The phase gradient k is extracted by correcting for 2π offsets and fitting a plane $\Phi(x,y) = k_x x + k_y y + \phi_0$. This long data acquisition procedure gives a reasonable signal to noise ratio, but it is undesirable for a sensor. In an optimized system, the phase gradient could be determined from three images by shifting the overall phase by $\pi/2$ between shots.

With this technique, k can be measured as a function of Ω. Then, the scale factor, F, can be estimated by fitting the data to $k = F\Omega$. By repeating this measurement for different initial distributions, the connection between the scale factor and the initial cloud size can be investigated. We consider a small cloud, produced by starting the optical molasses right after the MOT, and a large cloud, produced by adding a free expansion of 3 ms between the end of the MOT stage and the start of the molasses. During these 3 ms, the cloud expands rapidly because the atoms have a temperature of $T \approx 220\,\mu K$ after the MOT stage. The molasses stage erases the correlation between the position and velocity that develops during this initial free expansion; we obtain a cloud with $T \approx 5\,\mu K$ and an increased initial size. Table I shows the estimated initial sizes and temperatures for these two clouds. The clouds are

TABLE I. Estimated initial cloud parameters obtained by measuring the cloud's expansion as a function of time. The cloud is modeled as a Gaussian density distribution with initial width σ_0 and a velocity distribution at temperature T. Uncertainties were estimated by repeated measurements.

	σ_y (μm)	T_y (μK)	σ_x (μm)	T_x (μK)
Small cloud	224±6	5.3±0.3	375±8	5.6±0.3
Large cloud	590±5	4.4±0.5	715±10	4.9±0.5

asymmetric because the "y" direction corresponds to the axis of our MOT coils.

Figure 2 shows an example of a k vs Ω measurement for the four initial distributions in Table I. In each case, the data are reasonably described by $k = F\Omega$, but F depends on the initial distribution.

The relationship between the cloud expansion and the scale factor can be evaluated by measuring F as a function of T_R. The results, shown in Fig. 3, are consistent with Eq. (6) in that F decreases as the size of the initial cloud increases, and F converges to the point source limit as the expansion time increases. However, Eq. (6) does not describe the measured scale factors quantitatively because the initial distributions show significant deviations from a Gaussian profile. This indicates that detailed knowledge of the initial phase space distribution is needed to accurately model the scale factor.

The spatial fringe contrast with $\Omega = 0$ is about 20%, and it decreases with increasing Ω. The contrast loss can be quantified in a model independent way by estimating $\Omega_{50\%}$, the rotation rate where the contrast has fallen to half of its initial value. Figure 4 shows $\Omega_{50\%}$ as a function of T_R. At each T_R, the spatial fringe contrast falls off faster as a function of Ω for the larger initial clouds. This indicates that the contrast loss in our experiment is dominated by the blurring effect due to the finite size of the initial distribution. In
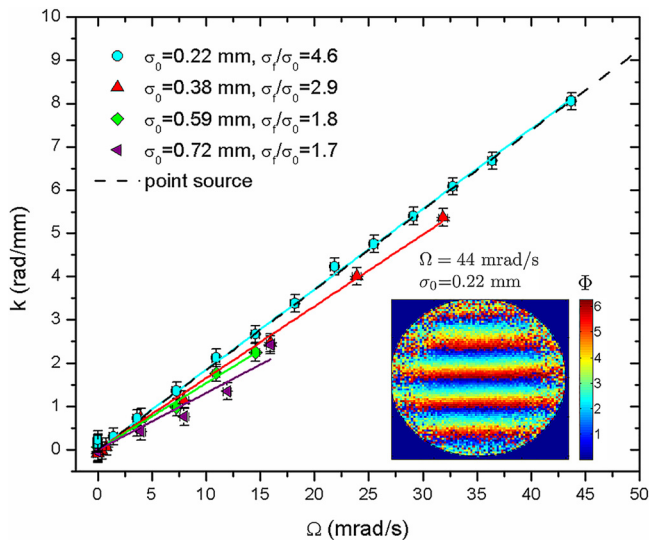

FIG. 2. Phase gradient k vs rotation rate Ω for different initial distributions with $T_R = 16$ ms. Solid lines are linear fits to the data used to estimate the scale factor F. An example of the phase maps used to estimate k is shown as an inset for $\Omega = 44$ mrad/s and $\sigma_0 = 0.22$ mm. The image is 4×4 mm. From repeated measurements, we estimate that the uncertainty in k is less than 0.2 rad/mm for all of our data.
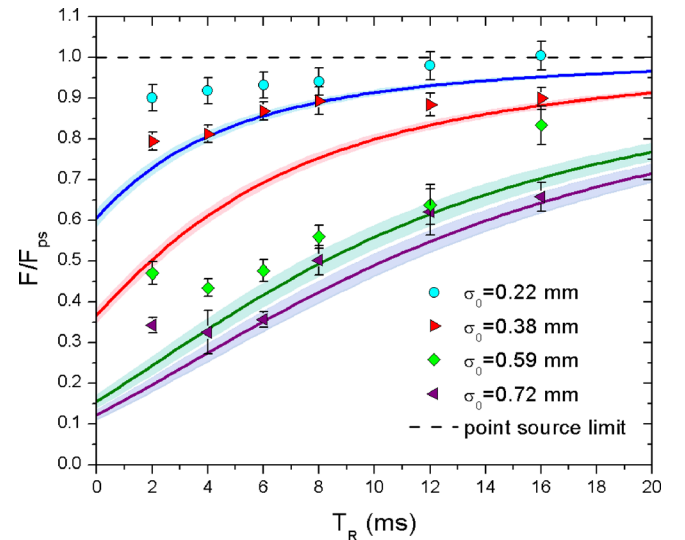

FIG. 3. Scale factor F/F_{ps} vs T_R for different initial distributions. Solid lines show the scale factor predicted by Eq. (6) for the initial cloud parameters in Table I. The shaded region around each curve represents the error from the uncertainty in σ_0 and T. The total expansion time is $T_{ex} = 2T_R + 12.3$ ms. The error bars are a quadratic sum of the uncertainties from the linear fits, the calibration of the imaging system magnification (1% error in F), and the calibration of the rotation rate (3% error in F).
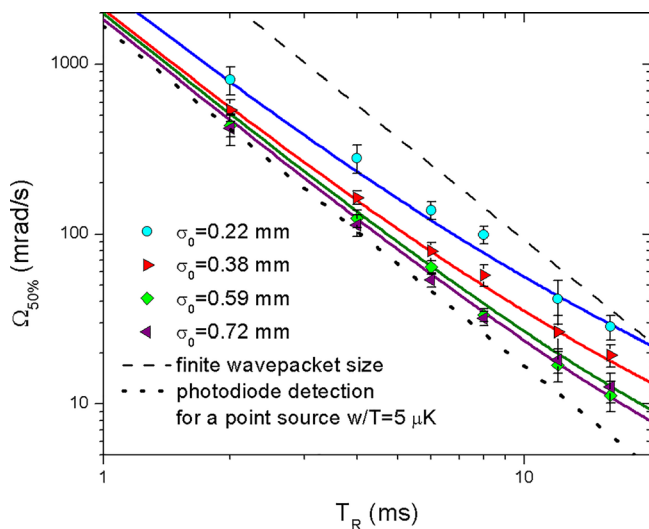
FIG. 4. $\Omega_{50\%}$ vs T_R for different initial distributions. To determine $\Omega_{50\%}$, we use spatially resolved fitting to find $c(\Omega)$. Then, linear interpolation is used to solve $c(\Omega)/c_0 = 0.5$ for each pixel. $\Omega_{50\%}$ is estimated by averaging over the cloud. The error bars indicate the spatial variation in $\Omega_{50\%}$. Solid lines show $\Omega_{50\%}$ predicted by Eq. (7) for the initial cloud parameters in Table I. The uncertainty in σ_0 and T leads to an error of about 3% in $\Omega_{50\%}$. The dashed line shows $\Omega_{50\%}$ for the contrast loss due to the imperfect overlap[17] of the atomic wave-packets during the final interferometer pulse for a wave-packet size $\lambda_{dB} = h/mv_{avg} \approx 130\,\text{nm}$ ($T = 5\,\mu\text{K}$). The dotted line shows $\Omega_{50\%}$ with a detection method that averages over the spatial fringes for a point source with $T = 5\,\mu\text{K}$.

addition to enabling rotation measurements with a single cloud, spatially resolved detection can also increase the dynamic range of LPAIs under rotation compared to the common strategy of averaging over the entire ensemble with a photodiode. For our smallest cloud and longest expansion time, we estimate that spatially resolved detection increases $\Omega_{50\%}$ by a factor of 4 compared to the contrast loss that would occur with a photodiode.

Finally, we emphasize that our result shows that the relationship between k and Ω in a PSI gyroscope will depend on the details of the initial atomic distribution in both position and velocity. In particular, the scale factor stability will depend on the stability of the initial distribution. This is a significant obstacle that must be overcome to realize a high-performance PSI gyroscope. One strategy that might be used to mitigate this difficulty is to control the initial distribution with a harmonic trapping potential. In this case, the initial cloud would be well described by a Gaussian density distribution and a temperature T. The expansion factor would

be $\sigma_f/\sigma_0 = \sqrt{1 + \omega_0^2 T_{ex}^2}$ where T_{ex} is the total expansion time and ω_0 is the trap frequency. The scale factor stability would depend on ω_0 and T_{ex} but not the cloud temperature T.

We have shown that PSI enables rotation measurements with a single cloud of cold atoms in the regime where the final cloud size is comparable to its initial size. The advantages offered by PSI in terms of sensor size and simplicity suggest that it is worthwhile to pursue PSI gyroscopes despite the challenges discussed here. In the short term, we plan to develop an optimized detection protocol and characterize the sensitivity of our current set up. In the long run, we hope to realize a compact, high-performance PSI gyroscope.

[1]A. D. Cronin, J. Schmiedmayer, and D. E. Pritchard, Rev. Mod. Phys. **81**, 1051 (2009).
[2]R. Geiger, V. Ménoret, G. Stern, N. Zahzam, P. Cheinet, B. Battelier, A. Villing, F. Moron, M. Lours, Y. Bidel, A. Bresson, A. Landragin, and P. Bouyer, Nat. Commun. **2**, 474 (2011).
[3]Y. Bidel, O. Carraz, R. Charrière, M. Cadoret, N. Zahzam, and A. Bresson, Appl. Phys. Lett. **102**, 144107 (2013).
[4]M. Hauth, C. Freier, V. Schkolnik, A. Senger, M. Schmidt, and A. Peters, Appl. Phys. B **113**, 49 (2013).
[5]T. Farah, C. Guerlin, A. Landragin, P. Bouyer, S. Gaffet, F. Pereira Dos Santos, and S. Merlet, Gyrosc. Navig. **5**, 266 (2014).
[6]X. Wu, Ph.D. thesis, Stanford University, 2009.
[7]K. Takase, Ph.D. thesis, Stanford University, 2008.
[8]M. A. Kasevich and S. Chu, Phys. Rev. Lett. **67**, 181 (1991).
[9]S. M. Dickerson, J. M. Hogan, A. Sugarbaker, D. M. S. Johnson, and M. A. Kasevich, Phys. Rev. Lett. **111**, 083001 (2013).
[10]T. L. Gustavson, A. Landragin, and M. A. Kasevich, Classical Quantum Gravity **17**, 2385 (2000).
[11]D. S. Durfee, Y. K. Saham, and M. A. Kasevich, Phys. Rev. Lett. **97**, 240801 (2006).
[12]B. Barrett, R. Geiger, I. Dutta, M. Meunier, B. Canuel, A. Gauguet, P. Bouyer, and A. Landragin, C. R. Phys. **15**, 875 (2014).
[13]G. Tackmann, P. Berg, S. Abend, C. Schubert, W. Ertmer, and E. M. Rasel, C. R. Phys. **15**, 884 (2014).
[14]A. V. Rakholia, H. J. McGuinness, and G. W. Biedermann, Phys. Rev. Appl. **2**, 054012 (2014).
[15]C. Jekeli, Navigation **52**, 1 (2005).
[16]S. Riedl, G. W. Hoth, B. Pelle, J. Kitching, and E. A. Donley, in Proceedings of the 8th Symposium on Frequency Standards and Metrology, Potsdam, Germany, 12–16 October 2015 [J. Phys.: Conf. Ser. **723**, 012058 (2016), available at http://iopscience.iop.org/article/10.1088/1742-6596/723/1/012058].
[17]S. Lan, P. Kuan, B. Estey, P. Haslinger, and H. Müller, Phys. Rev. Lett. **108**, 090402 (2012).
[18]H. J. McGuinness, A. V. Rakholia, and G. W. Biedermann, Appl. Phys. Lett. **100**, 011106 (2012).